https://dx.doi.org/10.1016/j.tws.2017.08.018
This is the Pre-Published Version.

Behaviours of concrete-filled cold-formed elliptical hollow section beam-columns with varying aspect ratios

Hua Yang[a,b], Faqi Liu[a,b,*], Tak-ming Chan[c], Wei Wang[a,b]

[a] Key Lab of Structures Dynamic Behavior and Control of the Ministry of Education, Harbin Institute of Technology, Harbin, 150090, China

[b] Key Lab of Smart Prevention and Mitigation of Civil Engineering Disasters of the Ministry of Industry and Information Technology, Harbin Institute of Technology, Harbin, 150090, China

[c] Department of Civil and Environmental Engineering, The Hong Kong Polytechnic University, Hong Kong, China

Abstract:

Experimental and numerical studies were conducted to investigate the behaviours of the concrete-filled cold-formed elliptical hollow section beam-columns. A total of 11 specimens were tested to evaluate the failure modes, load-deformation histories and strains development in the steel tube. Complementary finite element (FE) models were developed and validated against experimental results. Validated FE methodology was then used to study the influence of key parameters, including aspect ratio, slenderness ratio, load eccentricity ratio, yield strength of steel, compressive strength of concrete and steel tube to concrete area ratio, on the load carrying capacity. As a result, the design method for elliptical concrete-filled steel tubular (CFST) columns in Chinese code - GB50936-2014 and the design method for circular CFST columns in EC4 were assessed to confirm their applicability for cold-formed elliptical CFST columns with aspect ratio ranging from 1.0 to 2.5.

Key words: Aspect ratio; beam-column; concrete-filled steel tubular (CFST) column; elliptical section

© 2017. This manuscript version is made available under the CC-BY-NC-ND 4.0 license http://creativecommons.org/licenses/by-nc-nd/4.0/

Nomenclature	
a	major axis outer radius
b	minor axis outer radius
A_c	cross-sectional area of concrete core
A_s	cross-sectional area of steel tube
D_e	equivalent diameter
e	Load eccentricity
E_c	Young's modulus of concrete
E_s	Young's modulus of steel
f_c	concrete cylinder strength
f_y	yield strength of steel
L	length of column
L_e	effective length of column
M	bending moment
N	axial force
t_s	wall thickness of the steel tube
α_s	steel tube to concrete area ratio, $\alpha_s=A_s/A_c$
λ	slenderness ratio
χ	buckling reduction factor

1. Introduction

Concrete-filled steel tubular (CFST) column is well known for its high load-carrying capacity and good ductility due to the complementary characteristics between outer steel tube and inner concrete: the steel tube provides confinement to the concrete, thereby enhancing the strength and ductility of concrete, while the inner concrete on the other hand delays or even prevents local buckling of the steel tube, which increases the efficiency of the steel tube. The cross-section shape of the CFST column is generally circular, square or rectangular. In recent years, elliptical shape has been introduced into structural engineering because of its aesthetic appearance and structural efficiency [1]. To date, Yang et al. [2], Zhao and Packer [3], Dai and Lam [4], Jamaluddin et al. [5] have studied the cross-section behaviour of the elliptical CFST columns. Sheehan et al. [6] investigated the behaviours of eccentrically loaded elliptical CFST stub columns. Dai and Lam [7], McCann et al. [8], Mahgub et al. [9] and Qiu et al. [10] studied the axially and eccentrically loaded slender elliptical CFST columns. Ali et al. studied the behaviour of elliptical CFST columns exposed to hydrocarbon fire [11, 12].

All the above studies used hot-finished elliptical hollow sections, and the steel tube to concrete area ratio ranges from 13.2% to 38.9%, most of which exceeds the common range of steel tube to concrete area ratio of CFST column (4% to 20%[13]). And all these sections have a constant aspect ratio of 2.0. However, aspect ratio is an essential parameter which will affect the structural performance. If the aspect ratio approximates to 1.0, its performance resembles to a circular section while with an increase in the aspect ratio, the behaviour would tend to be similar to a rectangular section [14]. The confinement effect of steel tube to concrete also varies correspondingly with the varying aspect ratio, which further affects the load-carrying capacity and ductility. The varying aspect ratio can be achieved by cold-forming the elliptical shape.

Recently, a few studies have been conducted on the concrete-filled cold-formed elliptical hollow sections. Uenaka [15] and Chan et al. [16] investigated the behavior of concrete-filled cold-formed elliptical hollow section stub columns. Ren et al. [17] tested the behaviours of concrete-filled cold-formed elliptical hollow section beams and columns. Uenaka and Tsunokake tested the concrete-filled cold-formed elliptical hollow section columns under pure bending [18] and combined bending and shear [19]. Espinos et al. [20] tested the ambient and fire behaivours of

eccentrically loaded concrete-filled cold-formed elliptical hollow section slender columns.

Table 1 summarzies the previous studies on the elliptical CFST columns, in which a is the major axis outer radius, b is the minor axis outer radius, t_s is the steel wall thickness, α_s is the area ratio of steel tube to concrete $=A_s/A_c$ (in which A_s and A_c is the cross-section area of steel tube and cross-section area of concrete, respectively), L is the column length and e is the load eccentricity.

To date, no study has been reported on the cold-formed elliptical CFST beam-columns with varying aspect ratios. The authors have been carrying research on the behaviours of cold-formed elliptical CFST columns with varying aspect ratios. The first phase of the research focuses on the cross-section behaviours of cold-formed elliptical CFST stub columns under axial compression with an aspect ratio ranging from 1.0 to 2.5. Findings have been summarised in [21]. This paper expands the studies to the cross-section and member behaviours of cold-formed elliptical CFST beam-columns with varying aspect ratios.

A total of 11 specimens were tested to illustrate the fundamental behaviours of the axially loaded and eccentrically loaded slender columns. In parallel, finite element (FE) modelling methodology was developed to validate the experimental findings. Calibrated FE modelling methodology was then employed for parametric studies. Collated structural performance experimental and FE test results were assessed against related design standards. These include the design approach for elliptical CFST columns in Chinese code GB 50936 [25], and the design method for equivalent circular CFST columns in EC4 [26]. Findings indicated both design approaches can yield reasonable predictions on the load-carrying capacity of the cold-formed elliptical CFST columns subjected to combined axial force and bending.

2. Experimental program

2.1 Background

Tests of 11 concrete-filled cold-formed elliptical hollow section beam-columns were conducted to investigate their fundamental behaviours. The key parameters were slenderness ratio, $\lambda=L_e/i$ (where L_e is the effective length and i is the radius of gyration, both about relevant buckling axis) and load eccentricity, e (=0, 25mm, 50mm). Details of the specimens are presented in Table 2. These specimens were labelled with key parameters. The first letter ‘S’ or ‘L’ denotes stub column or long column, the second letter ‘Mi’ or ‘Ma’ (if any) stands for buckling about the minor axis or major

axis respectively, the next digits refer to the slenderness ratio about the corresponding axis, and the last digits are the load eccentricity (e) in mm. The steel tube to concrete area ratio was designed as 8.0% in the test. Influence of aspect ratio on the cross-section behaviour of elliptical CFST columns was investigated and presented in the complementary studies [21]. While in the present test programme, the aspect ratio, a/b was designed as 2.0 and its influence will be examined through numerical analysis.

The elliptical steel tubes were cold-formed from steel sheets with a nominal thickness of 2.75 mm and were seam welded. The steel tubes were fabricated with the same batch of sheets as the specimens tested in [21]. The properties of the steel were obtained by conducting tensile coupon tests according to ISO 6892-1 [22] and reported in [21]. The average yield strength and ultimate tensile strength are 376.4 N/mm^2 and 464.9 N/mm^2, respectively, and the elastic modulus is 1.85×10^5 N/mm^2 [21]. To examine the compressive strength and modulus of elasticity of the concrete, 150 mm ×150 mm ×150 mm cubes and 150 mm ×150 mm ×300 mm prisms were prepared and cured under the same condition as test specimens. The concrete cube compressive strength and elastic modulus were 57.3 N/mm^2 and 2.96×10^4 N/mm^2, respectively, at the test day.

2.2 Test setup and procedure

Tests were conducted using a 5000 kN hydraulic compression machine. The axially loaded stub column was centrally placed in the compression machine and loaded to failure (Fig.1 (a)). For other specimens, the pinned end condition was achieved by combining a knife edge and a grooved steel plate [23]. Therefore the specimens were only able to rotate about one axis. The effective length of specimens includes the length of steel tube (L), the thickness of the end plate (10 mm) and the thickness of the grooved steel plate (55.2 mm). Therefore the effective length of specimens $L_e = L + 2 \times 10$ mm $+ 2 \times 55.2$ mm (also shown in Table 2). For the axially loaded stub column, the axial displacements were measured during the loading process. For other columns, the lateral displacements were also measured. Strain gauges were placed in the longitudinal direction and transverse direction at the mid-height of the column to obtain corresponding strains. Loading setup and layout of instrumentations are presented in Fig.1.

2.3 Test results and discussions

Fig.2 shows failure modes of these specimens. The axially loaded stub column failed by shear

failure, consistent with observations in the previous study [21]. The eccentrically loaded stub columns failed by local buckling of the steel tube at the compression side accompanied by concrete crushing. While the axially loaded and eccentrically loaded slender columns failed by global buckling, and local buckling was also observed in the compression region at mid-height of some specimens. Though crushing of concrete occurred in some specimens, the inner concrete maintained intact, which can be attributed to the confinement effect of steel tube.

Fig. 3 shows the load versus deformation curves of the specimens. As anticipated, the load-carrying capacity of the elliptical CFST columns decreases with the increase in load eccentricity. Assessing the stub column specimens S-8, for example, the load-carrying capacity of the column with 25 mm and 50 mm eccentricity decreases by 24.7% and 44.4%, respectively, relative to that of the axially loaded stub column.

The influences of slenderness ratio on the load-lateral deformation curves are shown in Fig.4. As anticipated, the load-carrying capacity significantly decreases with the increase of slenderness ratio. Assessing the specimens with a load eccentricity of 25 mm for example, the load-carrying capacity decreases by 15.6% and 29.7% for columns with slenderness ratio of 35 and 50, respectively, relative to that of the stub column (λ=8).

The influences of buckling axis on the load-lateral deformation curves are presented in Fig.5. The slenderness ratio of the column buckling about major axis is about half of that of the column buckling about the minor axis. The load-carrying capacity of the former condition is 1.42 and 1.57 times of the latter condition, respectively, for the columns with an effective length L_e, of 1910.4 mm and 2670.4 mm. This different directional strength can provide efficient design while different strengths are required in two perpendicular axes.

The typical load-longitudinal strain curves of the concrete-filled elliptical hollow sections are illustrated in Fig.6. The whole cross-section is under compression during the loading process and the longitudinal strain distribution is pretty uniform for the stub column subjected to axial loaded (Fig.6(a)). For the axially loaded slender column, the whole cross-section is under compression before the peak load. However, part of the cross-section changes to be in tension from in compression during the post-peak phase, due to the second order effect. As expected, the larger is the load eccentricity, the earlier the tension region appears, as shown in Fig.6(b) to (d).

3. Finite element (FE) analysis

3.1 FE model

A finite element (FE) model was developed with program ABAQUS to further study the behaviour of the concrete-filled cold-formed elliptical hollow section beam-columns. The concrete damaged plasticity model was adopted for the concrete, which considers the degradation of the elastic stiffness both in tension and compression. The compressive stress-strain relationship for concrete in elliptical CFST columns [21] was employed and is given as follow:

$$y = \begin{cases} 2x - x^2 & x \le 1 \\ \dfrac{x}{\beta_0 (x-1)^2 + x} & x > 1 \end{cases} \tag{0}$$

in which $x = \varepsilon / \varepsilon_0$, $y = \sigma / \sigma_0$, $\xi = f_y A_s / f_{ck} A_c$, $\sigma_0 = f_c$, $\varepsilon_0 = \varepsilon_c + 800\xi^{0.2} \times 10^{-6}$, $\varepsilon_c = (1300 + 12.5 f_c) \cdot 10^{-6}$, $\beta_0 = (2.36 \times 10^{-5} \times (\mathrm{a/b})^5)^{[0.25+(\xi-0.5)^7]} \cdot (f_c)^{0.5} \cdot 0.5 \ge 0.12$, where f_y is the yield strength of the steel tube, A_s and A_c are the cross-sectional areas of the steel tube and the concrete, respectively, f_{ck} is the characteristic concrete strength and equals 0.67 times the concrete cube strength (f_{cu}), and f_c is the concrete cylinder strength. The initial elastic modulus was taken as $4700\sqrt{f_c}$ N/mm^2, according to the ACI specification[24].

A linear stress-strain relationship during both the ascending and descending phases [25] were employed for concrete in tension. A five-stage elastic-plastic stress-strain relationship [26] was adopted for both hot-finished steel and cold-formed steel. This stress-strain relationship model was compared with the multi-linear stress-strain model proposed by Abdel-Rahman and Sivakumaran [27] for analysis of cold-formed steel members. These two models are very close except some differences at the yield plateau and the fifth stage of the five-stage elastic-plastic model (corresponding strain exceeds 0.1), as shown in Fig.7. Influence of these differences between two models on the CFST columns is decreased by the infilled concrete. Therefore the same stress-strain relationship model is used for both hot-finished and cold-formed steel in elliptical CFST columns.

The steel tube and inner concrete were modelled with 4-noded shell element with reduced integration S4R and 8-noded solid element with reduced integration C3D8R, respectively. The interactive behaviour between the steel tube and concrete was defined with the interaction

algorithm in ABAQUS. The inner surface of steel tube and outer surface of the concrete were defined to be a contact pair, of which the former as slave surface and the latter as master surface. The behaviours of the interaction were defined with “hard” contact model in the normal direction and Coulomb friction model in the tangential direction. The friction coefficient was defined as 0.3 [25]. For the slender columns, the initial geometric imperfection was taken into account by performing the buckling analysis. The first buckling mode shape multiplied by an amplification factor of $L/1000$ was defined as the initial imperfection [23] , where L is the length. For CFST columns, the influences of residual stress and local imperfection are negligible due to the in-filled concrete [21, 28], therefore they were not considered in the FE model.

3.2 Verification of the FE model

The tested elliptical CFST columns in this study were predicted with the developed FE model, and the comparisons between the FE and test results are presented in Fig.8. Comparisons between FE and test load-bearing capacities are presented in Table 3. Besides, the slender elliptical CFST columns tested by Jamaluddin et al. [5], McCann et al. [8] and Ren et al. [17] were also predicted with the developed FE model. The comparisons between the predicted and test load-displacement curves are shown in Fig.9. Generally the developed FE model can reasonably predict the trends of the load-displacement curves of the elliptical CFST columns. Discrepancies of load-bearing capacity between FE results and test results may be resulted from deviations of initial imperfections and material properties in the test and FE model, and potential errors of the experimental tests. For some specimens (e.g. Fig.9(d) and (e)), there are also some discrepancies between test and predicted stiffness in the initial loading phase. This may be due to that a small eccentricity was not introduced in these axially loaded specimens and these columns buckled towards one direction but reverse to another during the loading process, which affects the measured initial stiffness. The comparisons between FE and test load-bearing capacities of the elliptical CFST columns with aspect ratio varying from 1.5 to 2.5 are presented in Fig.10, including stub columns in [21]. The mean and standard deviation of the ratio of the FE results to test results of the 67 specimens are 0.952 and 0.087, respectively, which confirms that the developed FE model can yield acceptable predictions of the axially loaded and eccentrically loaded slender elliptical CFST columns.

3.3 Parametric studies

After validating the FE modelling methodology, parametric studies were carried out to extend the range of the aspect ratio (a/b). The cross-section area maintains constant while the aspect ratio varies from 1.0 to 2.5.

The behaviour of a beam-column can be described by the load-moment (N-M) interaction curve, which includes the axial compression state (M=0), the pure bending state (N=0) and combined compression and bending state ($N\neq0$, $M\neq0$). The moments of eccentrically loaded columns were obtained by $M=N$ ($e+\delta_0+\delta$), in which N is the peak load, e is the load eccentricity, δ_0 is the initial imperfection, taken as $L/1000$, δ is the lateral deformation at mid-height of column corresponding to peak load. The influence of the aspect ratio on the load-moment interaction curves is shown in Fig.11. For the column fails by buckling about major axis (y-y), the axial compression load-carrying capacity and pure bending capacity decrease with the increase of aspect ratio, owning to the reduction of confinement of steel tube to concrete. For the column with large load eccentricity, the column with larger aspect ratio possesses better performance, which can be attributed to the increase of flexural stiffness with the increase of aspect ratio. However, the axial compression load-carrying capacity, pure bending capacity and combined axial compression and bending capacity decrease with the increase of aspect ratio when column buckles about minor axis (z-z).

4. Design method

Among the current design codes on CFST columns, only Chinese code GB50936 [29] covers the design of elliptical CFST columns. Liu et al. [21] noted that the cross-section capacity of elliptical CFST columns can be reasonably predicted with the method provided by GB50936, or by the method in EC4 [30] for circular CFST columns, with the use of an equivalent diameter. The method for elliptical CFST beam-columns in code GB50936 and related methods for CFST beam-columns in EC4 are assessed herein to evaluate their applicability for elliptical CFST beam-columns.

4.1 Code GB50936

Buckling capacity of the axially loaded slender column:

$$N_u = \chi f_{sc}(A_s + A_c) \tag{1}$$

where

$$\chi = \frac{1}{2\bar{\lambda}_{sc}^2}\left[\bar{\lambda}_{sc}^2 + \left(1 + K\bar{\lambda}_{sc}\right) - \sqrt{\left(\bar{\lambda}_{sc}^2 + \left(1 + K\bar{\lambda}_{sc}\right)\right)^2 - 4\bar{\lambda}_{sc}^2}\right] \tag{2}$$

$$\bar{\lambda}_{sc} = \left(\lambda / \pi\right)\sqrt{\frac{f_{sc}}{E_{sc}}} \tag{3}$$

$$E_{sc} = \left[\left(0.192\, f_y / 235 + 0.488\right) / \left(0.67\, f_y\right)\right] E_s\, f_{sc} \tag{4}$$

$$f_{sc} = (1.212 + B\xi + C\xi^2)\, f_c^{'} \tag{5}$$

$$B = (0.176\, f_y / 213 + 0.974)(\frac{b}{a})^{0.3} \tag{6}$$

$$C = (-0.104\, f_c / 14.4 + 0.031) \times (\frac{b}{a})^{0.3} \tag{7}$$

$$\alpha_s = \frac{A_s}{A_c} \tag{8}$$

$$\xi = \alpha_s \frac{f_y}{f_c} \tag{9}$$

in which χ is the buckling reduction factor, f_{sc} is the compressive strength of the composite member, $\bar{\lambda}_{sc}$ is the relative slenderness ratio, E_{sc} is the modulus of elasticity of the composite member, f_y is the yield strength of steel and $f_c^{'}$ is concrete prismatic strength. Yu [31] found that the buckling curve from Eq.(2) agrees well with the buckling curve "a" of EC3 [32] when K=0.16, therefore the factor K was taken as 0.16 in this study.

Flexural capacity of the column subjected to pure bending:

$$M_u = \gamma_m W_{sc}\, f_{sc} \tag{10}$$

where

$$\gamma_m = -0.483 k_e \xi + 1.926\sqrt{k_e \xi} \tag{11}$$

$$k_e = \begin{cases} \left(\alpha/b\right)^{0.12} & \text{about minor axis} \\ \left(b/a\right)^{0.6} & \text{about major axis} \end{cases} \tag{12}$$

$$W_{sc} = \begin{cases} \pi\alpha b^2/4 & \text{about minor axis} \\ \pi\alpha^2 b/4 & \text{about major axis} \end{cases} \tag{13}$$

Load-carrying capacity of the column under combined axial compression and bending:

When $\frac{N}{N_u} \geq 0.255$

$$\frac{N}{N_u} + \frac{\beta_m M}{1.5 M_u \left(1 - 0.4 \frac{N}{N_E^{'}}\right)} \leq 1 \tag{14}$$

When $\frac{N}{N_u} < 0.255$

$$-\frac{N}{2.17 N_u} + \frac{\beta_m M}{M_u \left(1 - 0.4 \frac{N}{N_E^{'}}\right)} \leq 1 \tag{15}$$

where

$$N_E^{'} = \frac{\pi^2 E_{sc} \left(A_s + A_c\right)}{1.1 \lambda^2} \tag{16}$$

in which N and M are applied axial force and bending moment, respectively, β_m is an equivalent moment factor, N_u and M_u are cross-section capacity and flexural capacity, respectively.

4.2 EC4

For circular CFST columns, the confinement effect on the strength of concrete may be considered when $\bar{\lambda} \leq 0.5$ and $e/d<0.1$. The cross-section capacity can be obtained as follows:

$$N_{pl,Rd} = \eta_s A_s f_y + A_c f_c \left(1 + \eta_c \frac{t_s}{d} \frac{f_y}{f_{ck}}\right) \tag{17}$$

where d is the cross-section diameter and f_{ck} is the characteristic value of cylinder compressive strength of concrete.

For members with $e=0$, the factor $\eta_s=\eta_{s0}$ and $\eta_c=\eta_{c0}$ are given as follows:

$$\eta_{s0} = 0.25\left(3 + 2\bar{\lambda}\right) \tag{18}$$

$$\eta_{c0} = 4.9 - 18.4\bar{\lambda} + 17\bar{\lambda}^2 \tag{19}$$

For members with $0<e/d\leqslant 0.1$, the factor η_s and η_c are given as follows:

$$\eta_s = \eta_{s0} + \left(1 - \eta_{s0}\right)\left(10 e/d\right) \tag{20}$$

$$\eta_c = \eta_{c0}\left(1 - 10 e/d\right) \tag{21}$$

For members with e/d>0.1, η_s=1.0 and η_c=0.

For elliptical sections, the diameter can be replaced by an equivalent diameter. For axial compression or bending about minor axis (z-z), $d_e=2(a^2/b)$; for bending about major axis (y-y), $d_e=2(b^2/a)$, for $a/b\leqslant 1.357$ and $d_e=0.8(a^2/b)$, for a/b>1.357 [33]. The area of concrete and steel tube can be calculated as follows:

$$A_c = \pi \cdot (a-t) \cdot (b-t) \tag{22}$$

$$A_s = \pi \cdot \left[a \cdot b - (a-t) \cdot (b-t) \right] \tag{23}$$

The buckling capacity of axially loaded slender columns can be determined as follows:

$$N_{Ed} = \chi N_{pl,Rd} \tag{24}$$

$$\chi = \frac{1}{\varphi + \sqrt{\varphi^2 - \bar{\lambda}^2}} \tag{25}$$

$$\varphi = 0.5\left[1 + \alpha\left(\bar{\lambda} - 0.2\right) + \bar{\lambda}^2 \right] \tag{26}$$

$$\bar{\lambda} = \sqrt{\frac{N_{pl,Rd}}{N_{cr}}} \tag{27}$$

$$N_{cr} = \frac{\pi^2 (EI)_{eff}}{L^2} \tag{28}$$

$$(EI)_{eff} = E_s I_s + 0.6 E_{cm} I_c \tag{29}$$

in which α is an imperfection factor, which was taken as 0.21, corresponding to buckling curve "a" of columns [5], E_s and E_{cm} are modulus of elasticity of steel tube and un-cracked concrete, respectively, I_s and I_c are second moments of area of steel tube and un-cracked concrete, respectively.

For column under combined axial compression and uniaxial bending:

$$\frac{M_{Ed}}{\mu_d M_{pl,Rd}} \leq \alpha_M \tag{30}$$

in which M_{Ed} is the greatest of the end moments and the maximum bending moment within the column length, taking into account imperfections and second order effects, $M_{pl,Rd}$ is the plastic bending capacity, α_M is a coefficient, which should be taken as 0.9 for steel grades S235 and S355,

and 0.8 for steel grades S420 and S460.

The first order bending moment M_{Ed} arising from initial imperfections and eccentric load is:

$$M_{\mathrm{Ed}} = N_{\mathrm{Ed}}\left(e_0 + e\right) \tag{31}$$

in which e is the load eccentricity, e_0 is the initial global imperfection, which should be taken as $L/300$ according to EC4. However, in this study, to be consistent with the FE results, global imperfection e_0 was taken as $L/1000$ while compared with FE results.

Second order effects can be considered by multiplying the first order moment M_{Ed} by a factor k, presented as follows:

$$k = \frac{\beta}{1 - N_{\mathrm{Ed}} / N_{\mathrm{cr,eff}}} \tag{32}$$

in which β is an equivalent moment factor, $N_{cr,eff}$ is the critical normal force for the relevant axis and corresponding to the effective flexural stiffness given in Eq.(33).

$$\left(EI\right)_{\mathrm{eff,II}} = 0.9\left(E_{\mathrm{s}} I_{\mathrm{s}} + 0.5 E_{\mathrm{cm}} I_{\mathrm{c}}\right) \tag{33}$$

For the column under combined axial compression and bending moment, a simplified *N-M* (minor axis z-z) interaction curve is shown in Fig.12. The load-carrying capacity corresponding to point B, C and D in Fig.12 can be calculated using stress block method [6]. The value μ_d can be interpolated according to Fig.12, given as follows:

For part AC, $N_{\mathrm{Ed}} > N_{\mathrm{pm,Rd}}$:

$$\mu_{\mathrm{d}} = \frac{M_{\mathrm{Ed}}}{M_{\mathrm{pl,Rd}}} = \frac{N_{\mathrm{pl,Rd}} - N_{\mathrm{Ed}}}{N_{\mathrm{pl,Rd}} - N_{\mathrm{pm,Rd}}} \tag{34}$$

For part CD, $N_{\mathrm{pm,Rd}}/2 < N_{\mathrm{Ed}} \le N_{\mathrm{pm,Rd}}$:

$$\mu_{\mathrm{d}} = \frac{M_{\mathrm{Ed}}}{M_{\mathrm{pl,Rd}}} = 1 + \frac{2\left(N_{\mathrm{pm,Rd}} - N_{\mathrm{Ed}}\right)}{N_{\mathrm{pm,Rd}}} \cdot \left(\frac{M_{\mathrm{max,Rd}}}{M_{\mathrm{pl,Rd}}} - 1\right) \tag{35}$$

For part DB, $N_{\mathrm{Ed}} \le N_{\mathrm{pm,Rd}}/2$:

$$\mu_{\mathrm{d}} = \frac{M_{\mathrm{Ed}}}{M_{\mathrm{pl,Rd}}} = 1 + \frac{2N_{\mathrm{Ed}}}{N_{\mathrm{pm,Rd}}} \left(\frac{M_{\mathrm{max,Rd}}}{M_{\mathrm{pl,Rd}}} - 1\right) \tag{36}$$

The FE results and predicted results of code GB50936 and EC4 are compared in Fig.13 and Fig.14,

respectively, in which μ and S are the mean and standard deviation of the ratio of predicted results to test results, respectively. Both of these two methods yield accurate predictions of the load-carrying capacity of the elliptical CFST columns under axial compression and pure bending, with a maximum deviation of 0.086 (shown in Fig.13 (a), (b) and Fig.14 (a), (b)). For elliptical CFST columns subjected to combined axial compression and bending, the method specified in GB50936 yields better predictions than that in EC4. The deviation of the prediction of the method specified in GB50936 is within 0.1, while that corresponding to EC4 is between 0.111 and 0.186, as shown in Fig.13 (c)-(f) and Fig.14 (c)-(f). Test specimens in this study and related studies were also predicted with above methods and are presented Fig.15. Based on these comparisons, it can be found that the above design methods can yield reasonable predictions of the load-carrying capacity of the cold-formed elliptical CFST beam-columns with aspect ratios ranging from 1.0 to 2.5.

5. Conclusions

Behaviour of concrete-filled cold-formed elliptical hollow section beam-columns with aspect ratios ranging from 1.0 to 2.5 was studied experimentally and numerically. Based on the structural performance data, the following conclusions can be drawn:

Elliptical CFST slender beam-columns failed by global buckling, and local buckling of steel tube can be observed on the compression side. The increase in the slenderness ratio and load eccentricity significantly reduces load-carrying capacity of the elliptical CFST beam-columns. Axial compression capacity and pure bending capacity decrease with the increase of aspect ratio, however, the combined axial compression and bending capacity can be enhanced with the increase of aspect ratio for columns failed by buckling about major axis and with large load eccentricity. Design method for elliptical CFST columns in code GB50936 and design method for circular CFST columns in code EC4 can be applied for elliptical CFST beam-columns with aspect ratio varying from 1.0 to 2.5, both of which can yield reasonable predictions.

6. Acknowledgement

The research presented in this paper was sponsored by the National Natural Science Foundation (No. 51508131) and Hei Long Jiang Postdoctoral Foundation (LBH-Z15086); their financial support is highly appreciated. The third author is also grateful for the support from the Chinese

National Engineering Research Centre for Steel Construction (Hong Kong Branch).

7. References

[1] Chan TM, Gardner L, Law KH. Structural design of elliptical hollow sections: a review. Proceedings of the ICE-Structures and Buildings. 2010;163:391-402.

[2] Yang H, Lam D, Gardner L. Testing and analysis of concrete-filled elliptical hollow sections. Engineering Structures. 2008;30:3771-81.

[3] Zhao XL, Packer JA. Tests and design of concrete-filled elliptical hollow section stub columns. Thin-Walled Structures. 2009;47:617-28.

[4] Dai X, Lam D. Numerical modelling of the axial compressive behaviour of short concrete-filled elliptical steel columns. Journal of Constructional Steel Research. 2010;66:931-42.

[5] Jamaluddin N, Lam D, Dai XH, Ye J. An experimental study on elliptical concrete filled columns under axial compression. Journal of Constructional Steel Research. 2013;87:6-16.

[6] Sheehan T, Dai XH, Chan TM, Lam D. Structural response of concrete-filled elliptical steel hollow sections under eccentric compression. Engineering Structures. 2012;45:314-23.

[7] Dai XH, Lam D, Jamaluddin N, Ye J. Numerical analysis of slender elliptical concrete filled columns under axial compression. Thin-Walled Structures. 2014;77:26-35.

[8] McCann F, Gardner L, Qiu W. Experimental study of slender concrete-filled elliptical hollow section beam-columns. Journal of Constructional Steel Research. 2015;113:185-94.

[9] Mahgub M, Ashour A, Lam D, Dai X. Tests of self-compacting concrete filled elliptical steel tube columns. Thin-Walled Structures. 2017;110:27-34.

[10] Qiu W, McCann F, Espinos A, Romero ML, Gardner L. Numerical analysis and design of slender concrete-filled elliptical hollow section columns and beam-columns. Engineering Structures. 2017;131:90-100.

[11] Ali F, Jeffers A, Goodfellow N, Nadjai A, Scullion T, Gardner J. Performance of Axially Restrained Hollow and Concrete Filled Oval Steel Columns Subjected to Hydrocarbon Fire. Journal of Structural Fire Engineering. 2012;3:181-98.

[12] Ali F, Nadjai A, Goodfellow N. Experimental and numerical study on the performance of hollow and concrete-filled elliptical steel columns subjected to severe fire. Fire and Materials. 2016;40:635-52.

[13] Zhong S. The Concrete-filled Steel Tubular Structures: Tsinghua University Press; 2003(in Chinese).

[14] Ruiz-Teran AM, Gardner L. Elastic buckling of elliptical tubes. Thin-Walled Structures. 2008;46:1304-18.

[15] Uenaka K. Experimental study on concrete filled elliptical/oval steel tubular stub columns under compression. Thin-Walled Structures. 2014;78:131-7.

[16] Chan T-M, Huai Y-M, Wang W. Experimental investigation on lightweight concrete-filled cold-formed elliptical hollow section stub columns. Journal of Constructional Steel Research. 2015;115:434-44.

[17] Ren Q-X, Han L-H, Lam D, Li W. Tests on elliptical concrete filled steel tubular (CFST) beams and columns. Journal of Constructional Steel Research. 2014;99:149-60.

[18] Uenaka K, Tsunokake H. Concrete filled elliptical steel tubular members with large diameter-to-thickness ratio subjected to bending. Structures. 2016;5:58-66.

[19] Uenaka K, Tsunokake H. Behavior of Concrete Filled Elliptical Steel Tubular Deep Beam under Bending-Shear. Structures. 2017;10:89-95.

[20] Espinos A, Romero ML, Portolés JM, Hospitaler A. Ambient and fire behavior of eccentrically loaded elliptical slender concrete-filled tubular columns. Journal of Constructional Steel Research. 2014;100:97-107.

[21] Liu F, Wang Y, Chan T-m. Behaviour of concrete-filled cold-formed elliptical hollow sections with varying aspect ratios. Thin-Walled Structures. 2017;110:47-61.

[22] ISO E. 6892-1 Metallic materials Tensile testing Part 1: Method of test at room temperature. International Organization for Standardization. 2009.

[23] Yang H, Liu F, Gardner L. Post-fire behaviour of slender reinforced concrete columns confined by circular steel tubes. Thin-Walled Structures. 2015;87:12-29.

[24] Committee American. Building code requirements for structural concrete (ACI 318-08) and commentary. American Concrete Institute; 2008.

[25] Liu F, Gardner L, Yang H. Post-fire behaviour of reinforced concrete stub columns confined by circular steel tubes. Journal of Constructional Steel Research. 2014;102:82-103.

[26] Han L-H, Yao G-H, Tao Z. Performance of concrete-filled thin-walled steel tubes under pure

torsion. Thin-Walled Structures. 2007;45:24-36.

[27] Abdel-Rahman N, Sivakumaran KS. Material properties models for analysis of cold-formed steel members. J Struct Eng-Asce. 1997;123:1135-43.

[28] Tao Z, Wang Z-B, Yu Q. Finite element modelling of concrete-filled steel stub columns under axial compression. Journal of Constructional Steel Research. 2013;89:121-31.

[29] GB 50936-2014. Technical code for concrete filled steel tubular structures. Ministry of Housing and Urban-Rural Development of the People's Republic of China. 2014.

[30] BS EN 1994-1-1: Eurocode 4. Design of composite steel and concrete structures Part 1-1: General rules and rules for buildings. London: British Standards Institution. 2004.

[31] Yu M, Zha X, Ye J, Li Y. A unified formulation for circle and polygon concrete-filled steel tube columns under axial compression. Engineering Structures. 2013;49:1-10.

[32] BS EN 1993-1-1: Eurocode 3. Design of steel structures Part 1-1: General rules and rules for buildings. London: British Standards Institution. 2005.

[33] Chan TM, Gardner L. Bending strength of hot-rolled elliptical hollow sections. Journal of Constructional Steel Research. 2008;64:971-86.

Figures captions

Table captions

(a)

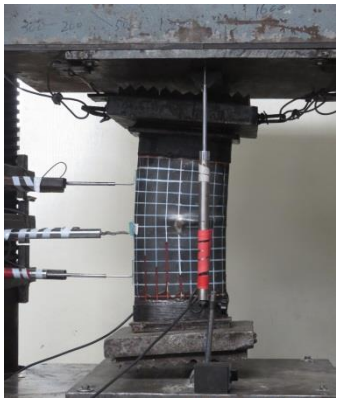

(b)

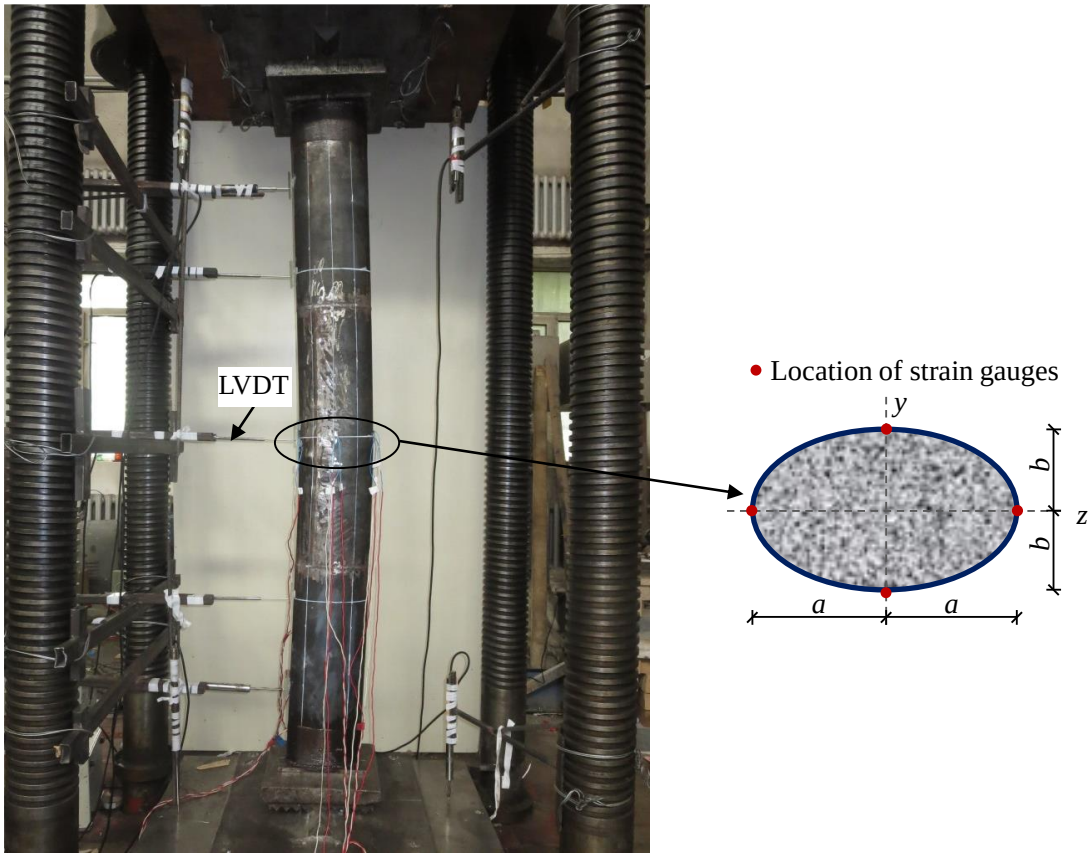

(c)

Fig.1 Loading setup and layout of instrumentations: (a) axially loaded stub column; (b) eccentrically loaded stub column; and (c) slender column.

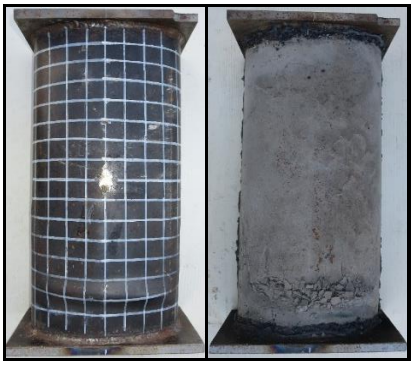

(a)

(b)

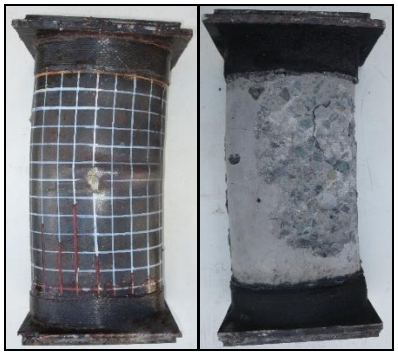

(c)

(d)

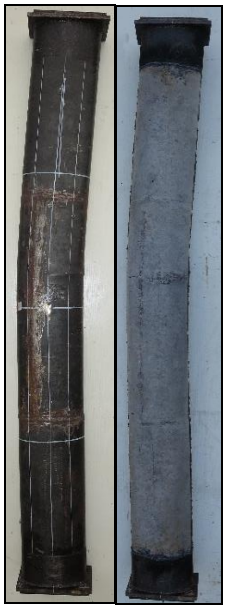

(e)

(f)

(g)

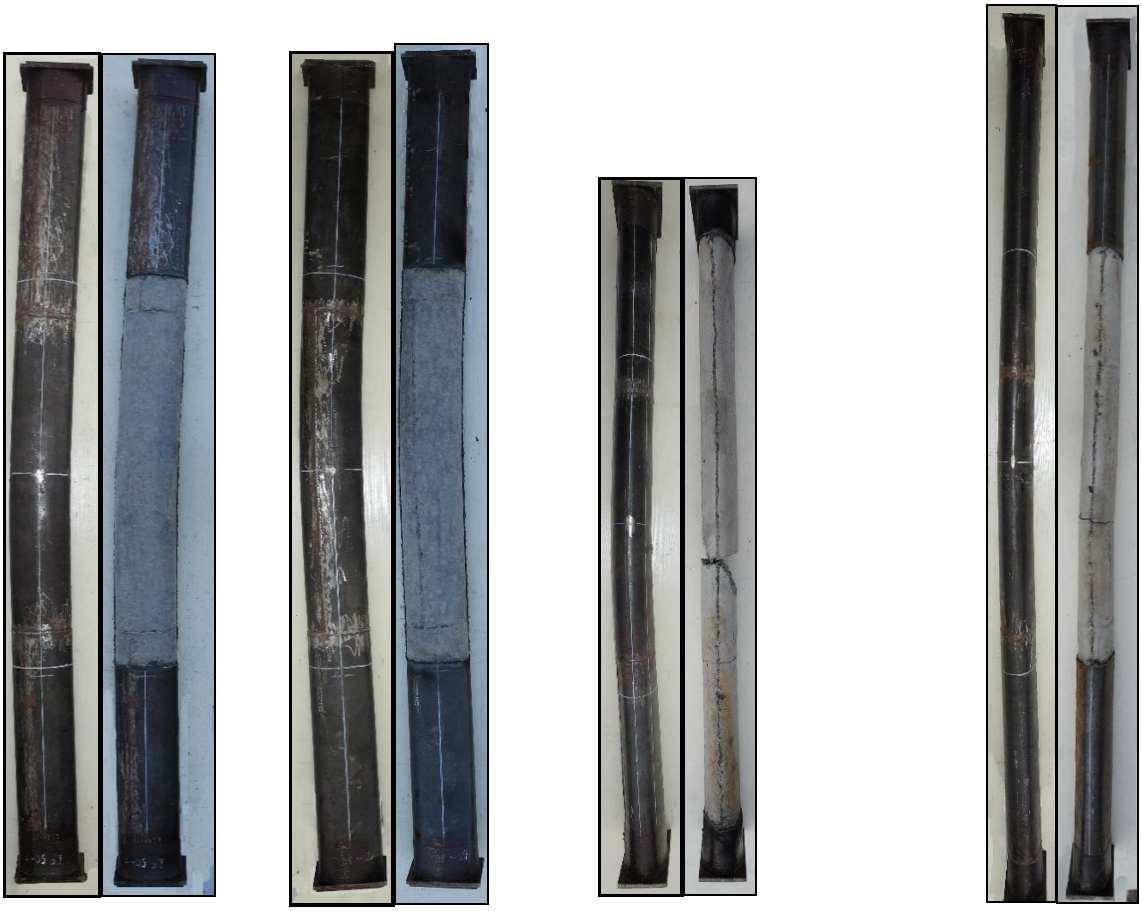

(h) (i) (j) (k)

Fig.2 Failure modes of specimens: (a) S-8-0; (b) S-8-25; (c) S-8-50; (d) L-Ma-35-0; (e) L-Ma-35-25; (f) L-Ma-35-50; (g) L-Ma-50-0; (h) L-Ma-50-25; (i) L-Ma-50-50; (j) L-Mi-70-0; and (k) L-Mi-100-0.

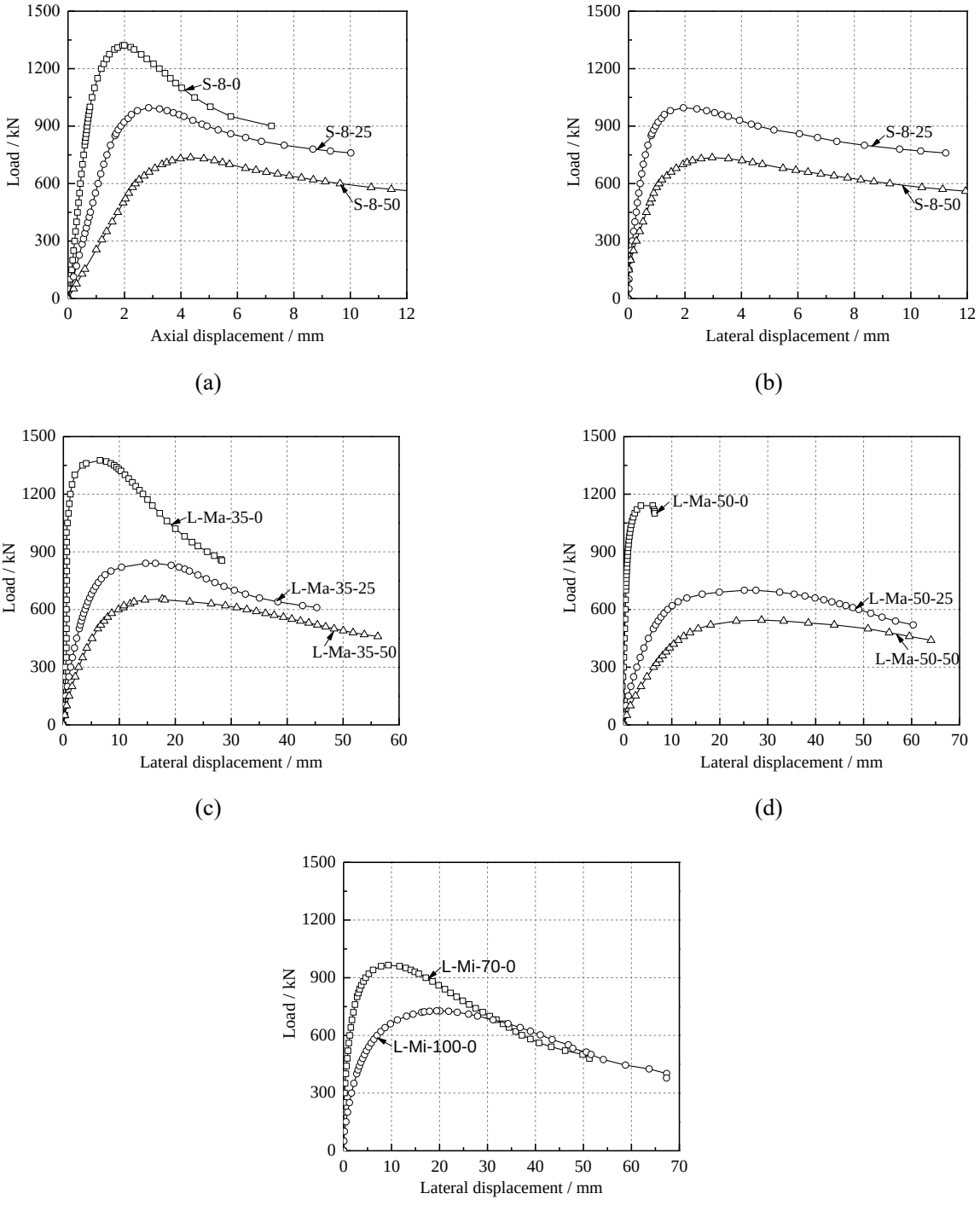

Fig.3 Load-displacement curves of test specimens: (a) S-8-0/25/50 (axial displacement); (b) S-8-25/50; (c) L-Ma-35-0/25/50; (d) L-Ma-50-0/25/50; and (e) L-Mi-70/100-0.

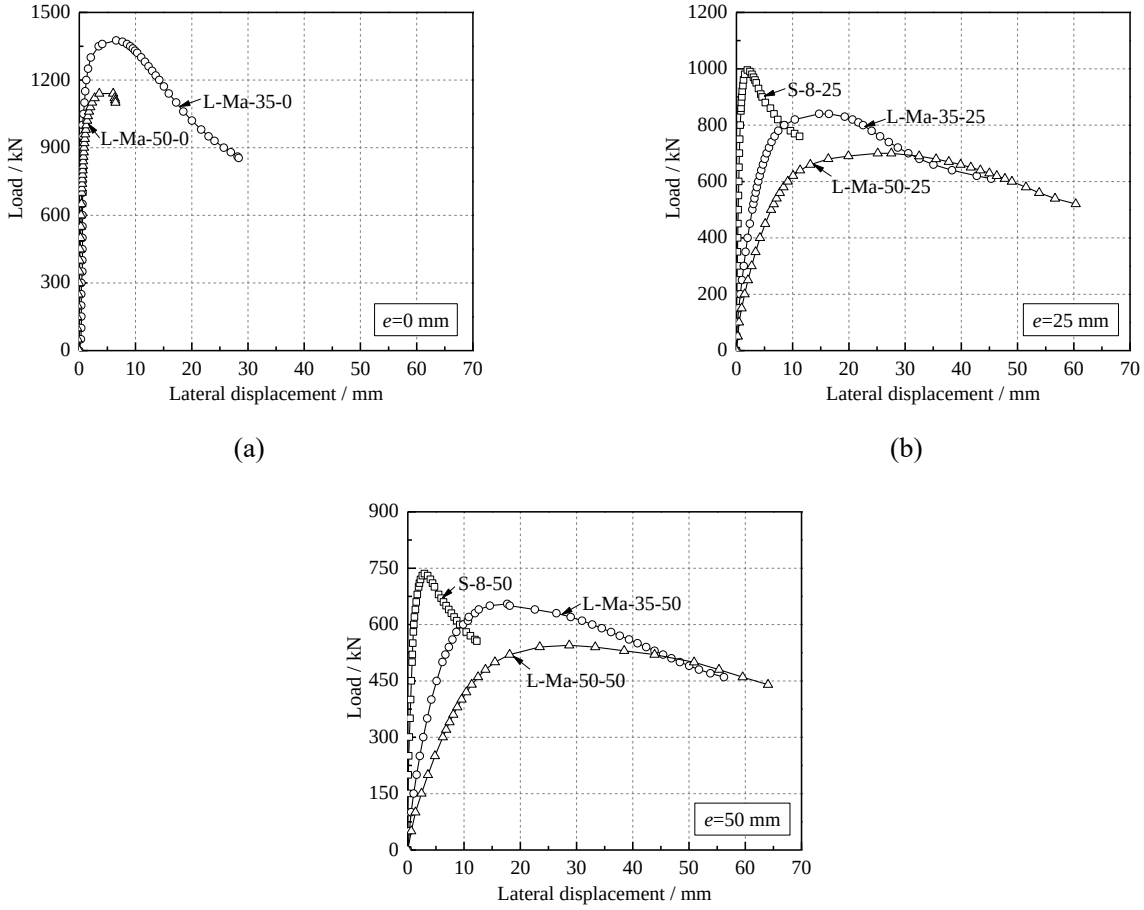

Fig.4 Influences of slenderness ratio on load-lateral displacement curves of test specimens: (a) *e*=0 mm; (b) *e*=25 mm; and (e) *e*=50 mm.

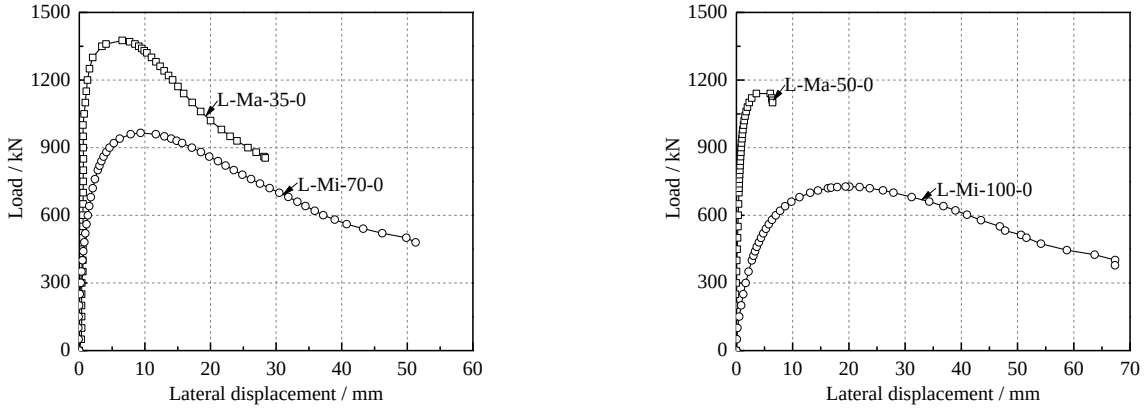

Fig.5 Influences of buckling axis on load-lateral displacement curves of test specimens: (a) L_e=1910.4 mm; and (b) L_e =2670.4 mm.

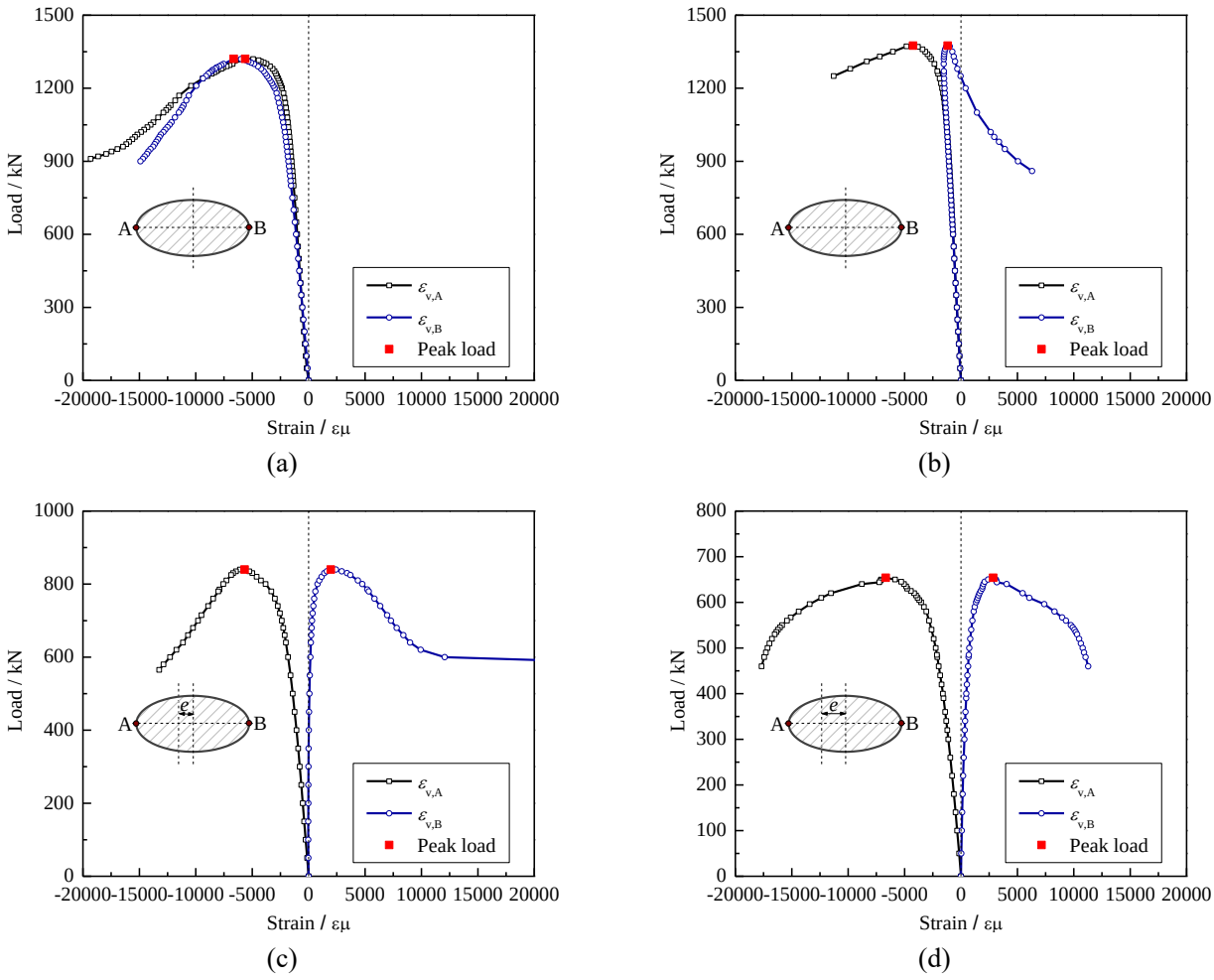

Fig.6 Load-longitudinal strain curves of specimens: (a) S-8-0; (b) L-Ma-35-0; (c) L-Ma-35-25; and (d) L-Ma-35-50.

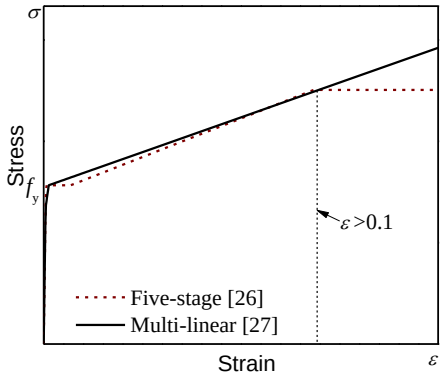

Fig.7 Stress-strain relationship model of steel

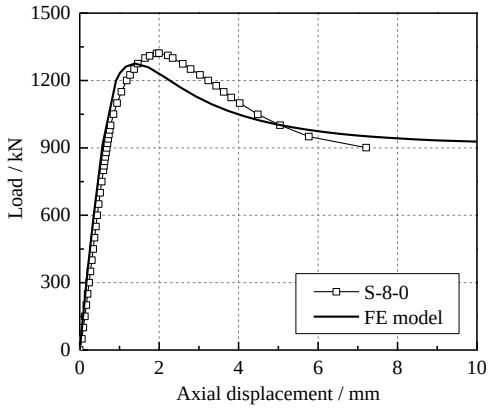
Load / kN
Axial displacement / mm
S-8-0
FE model

(a)

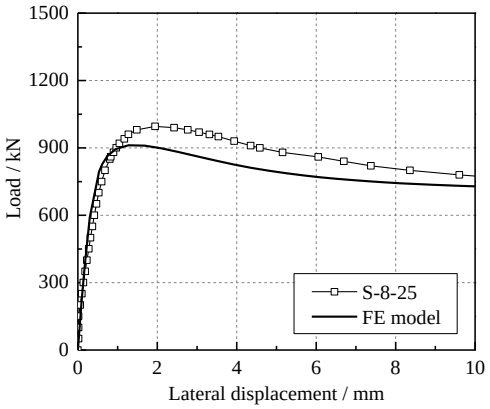
Load / kN
Lateral displacement / mm
S-8-25
FE model

(b)

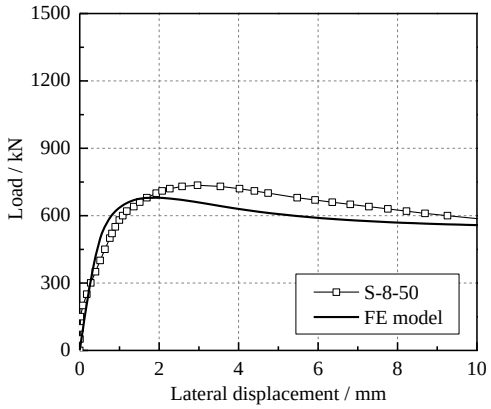
Load / kN
Lateral displacement / mm
S-8-50
FE model

(c)

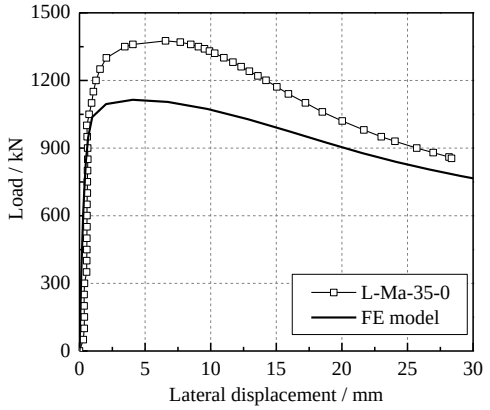
Load / kN
Lateral displacement / mm
L-Ma-35-0
FE model

(d)

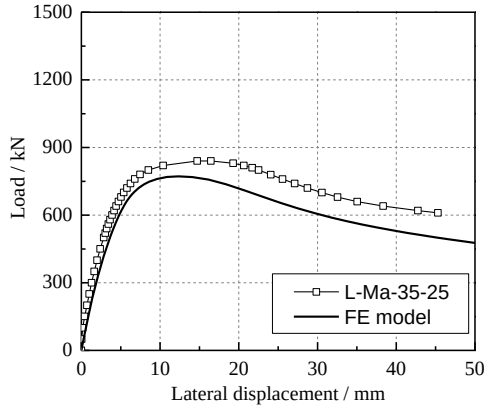
Load / kN
Lateral displacement / mm
L-Ma-35-25
FE model

(e)

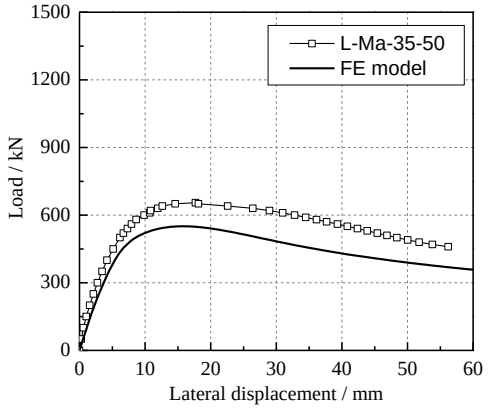
Load / kN
Lateral displacement / mm
L-Ma-35-50
FE model

(f)

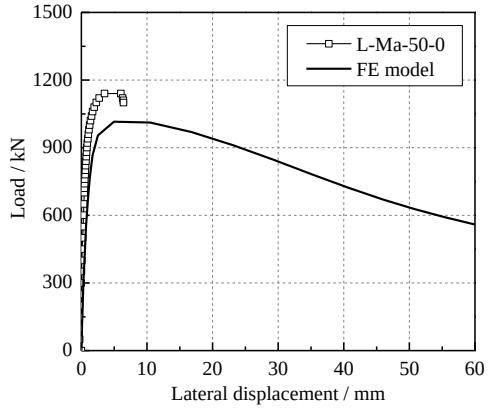

(g)

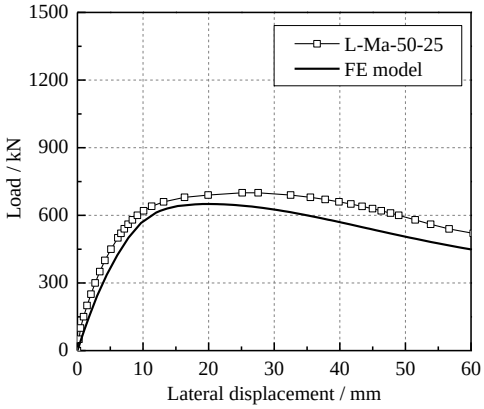

(h)

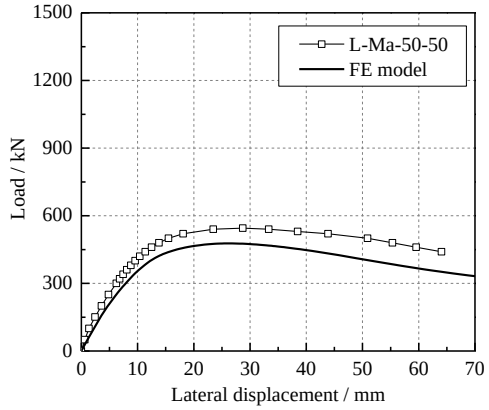

(i)

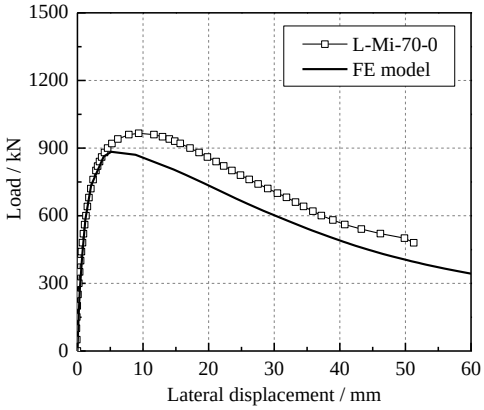

(j)

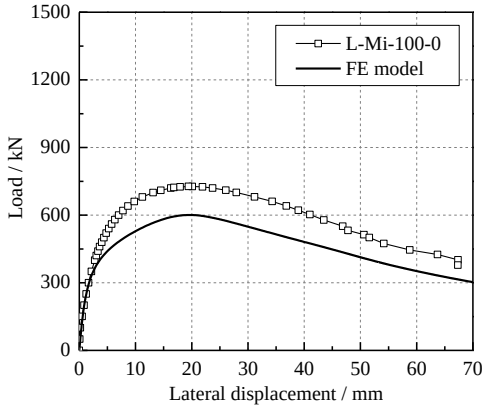

Fig.8 Comparisons between predicted and test load-deformation curves: (a) S-8-0; (b) S-8-25; (c) S-8-50; (d) L-Ma-35-0; (e) L-Ma-35-25; (f) L-Ma-35-50; (g) L-Ma-50-0; (h) L-Ma-50-25; (i) L-Ma-50-50; (j) L-Mi-70-0; and (k) L-Mi-100-0.

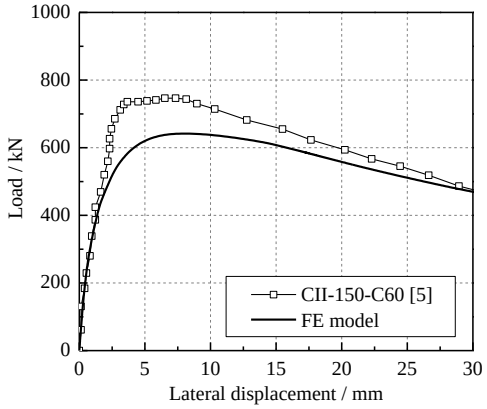
Load / kN
Lateral displacement / mm
CII-150-C60 [5]
FE model

(a)

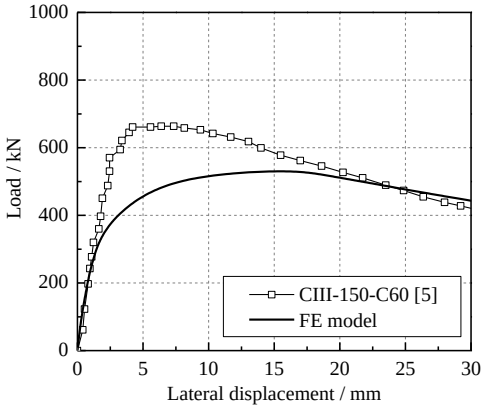
Load / kN
Lateral displacement / mm
CIII-150-C60 [5]
FE model

(b)

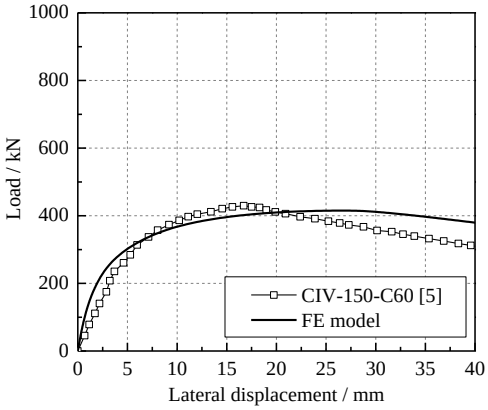
Load / kN
Lateral displacement / mm
CIV-150-C60 [5]
FE model

(c)

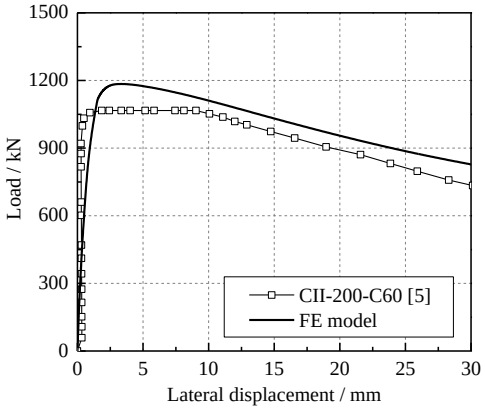
Load / kN
Lateral displacement / mm
CII-200-C60 [5]
FE model

(d)

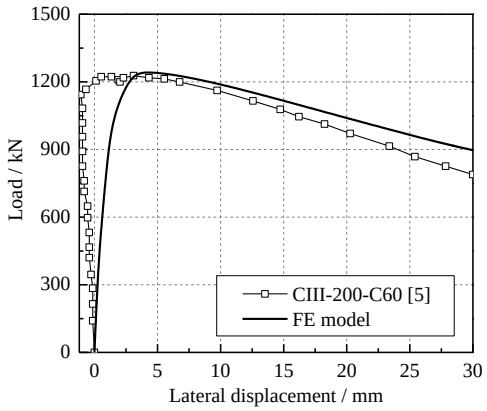
Load / kN
Lateral displacement / mm
CIII-200-C60 [5]
FE model

(e)

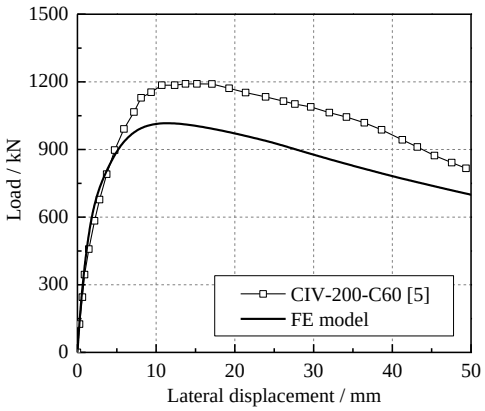
Load / kN
Lateral displacement / mm
CIV-200-C60 [5]
FE model

(f)

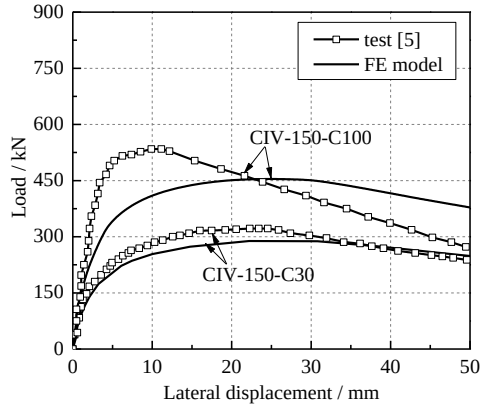
test [5]
FE model
CIV-150-C100
CIV-150-C30
Load / kN
Lateral displacement / mm

(g)

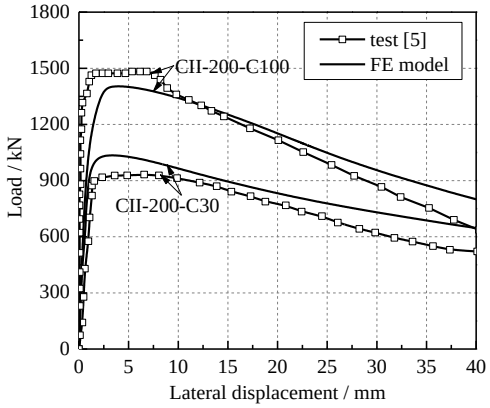
test [5]
FE model
CII-200-C100
CII-200-C30
Load / kN
Lateral displacement / mm

(h)

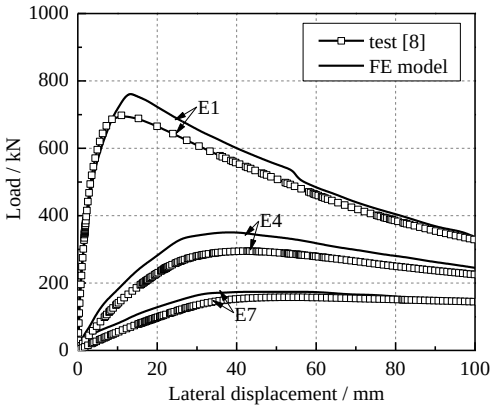
test [8]
FE model
E1
E4
E7
Load / kN
Lateral displacement / mm

(i)

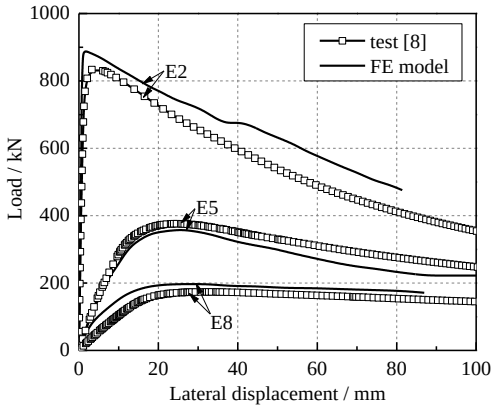
test [8]
FE model
E2
E5
E8
Load / kN
Lateral displacement / mm

(j)

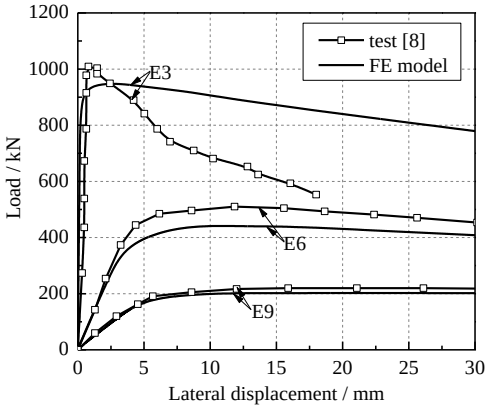
test [8]
FE model
E3
E6
E9
Load / kN
Lateral displacement / mm

(k)

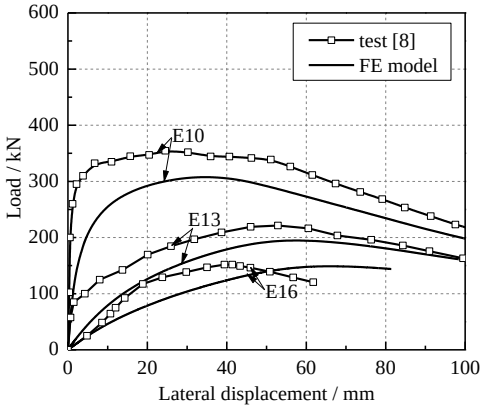
test [8]
FE model
E10
E13
E16
Load / kN
Lateral displacement / mm

(m)

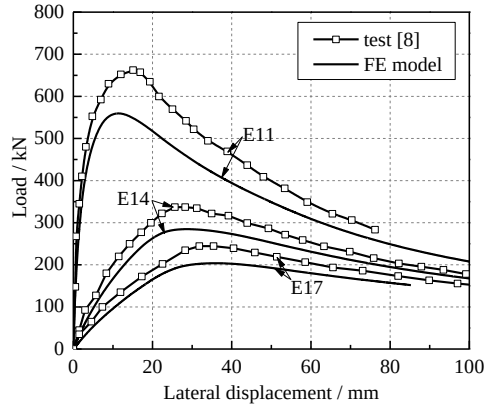

(n)

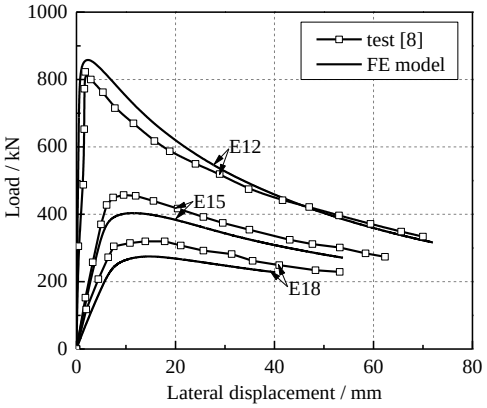

(o)

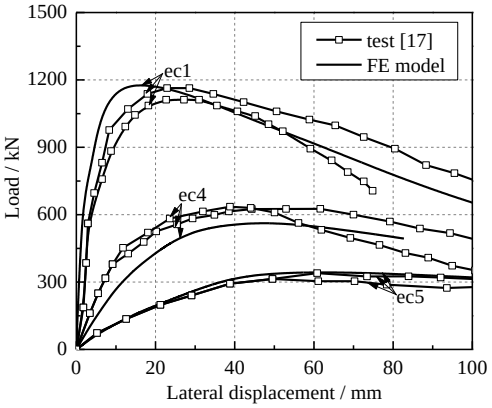

(p)

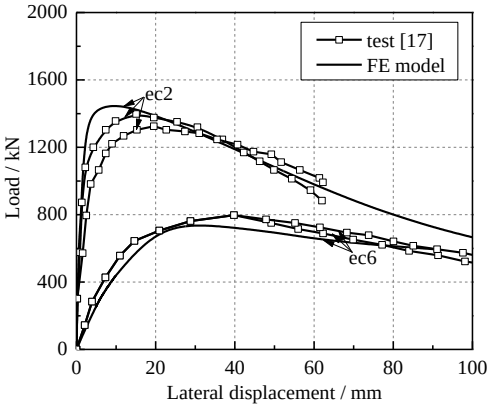

(q)

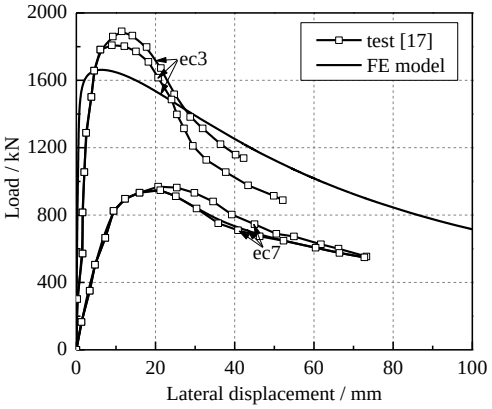

(r)

Fig.9 Typical comparisons between predicted and test load-deformation curves: (a) CII-150-C60; (b) CIII-150-C60; (c) CIV-150-C60; (d) CII-200-C60; (e) CIII-200-C60; (f) CIV-200-C60; (g) CIV-150-C30/C100; (h) CII-200-C30/C100; (i) E1/4/7; (j) E2/5/8; (k) E3/6/9; (m) E10/13/16; (n) E11/14/17; (o) E12/15/18; (p) ec1/4/5; (q) ec2/6; and (r) ec3/7.

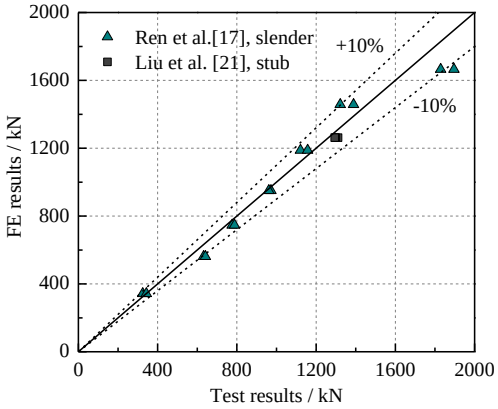

(a)

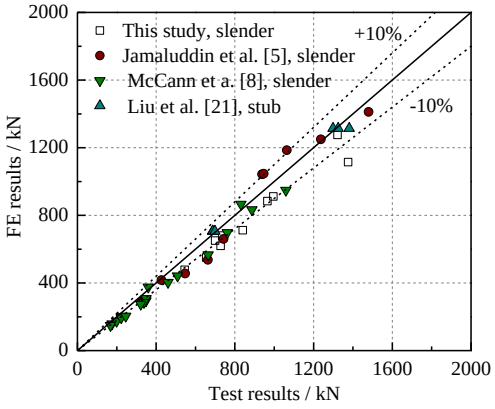

(b)

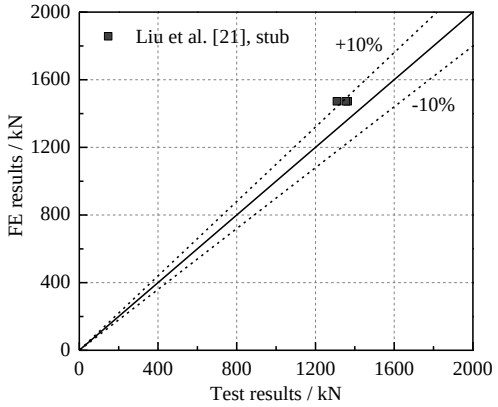

(c)

Fig.10 Comparisons between predicted and test load-carrying capacities: (a) a=1.5b; (b) a=2.0b; and (c) a=2.5b.

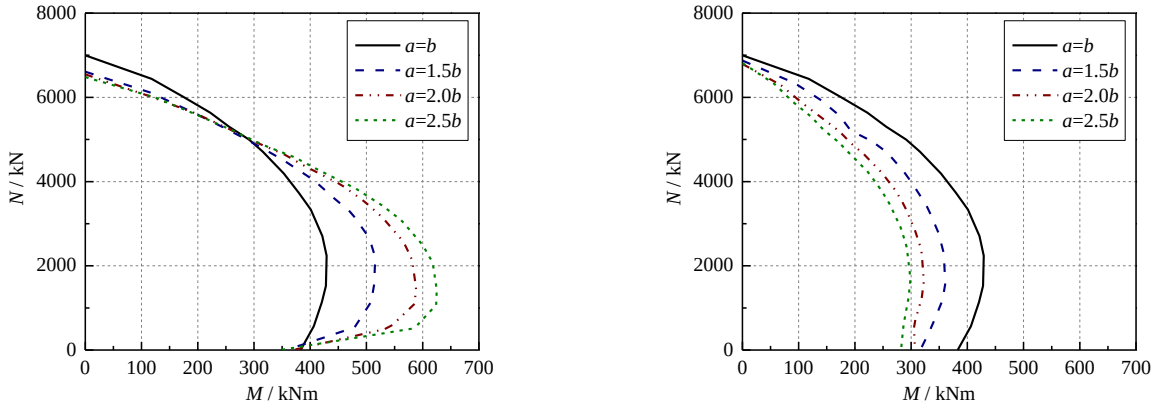

Fig.11 Influence of aspect ratio on the *N*-*M* interaction curve about: (a) major axis; and (b) minor axis.

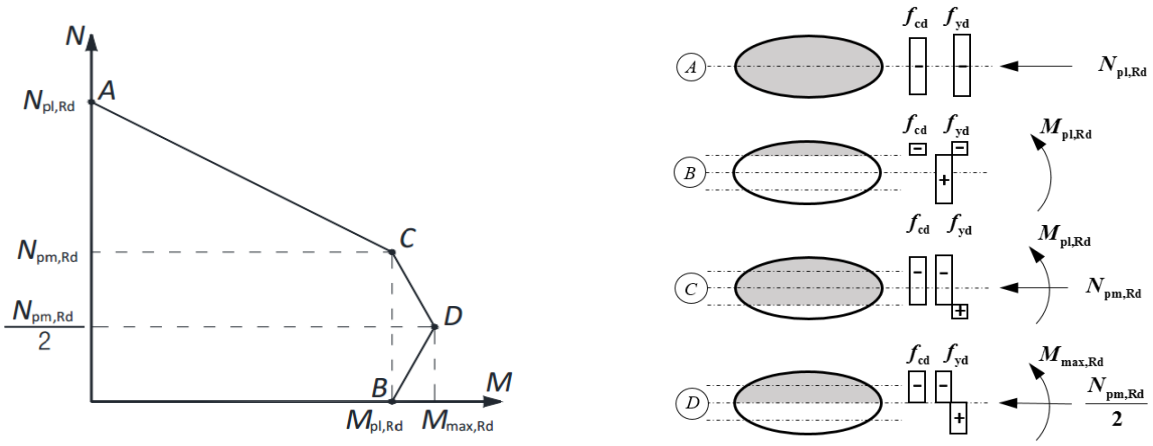

(a) (b)

Fig.12 Simplified N-M (minor axis, z-z) interaction curve and stress distribution: (a) interaction curve; and (b) stress distribution.

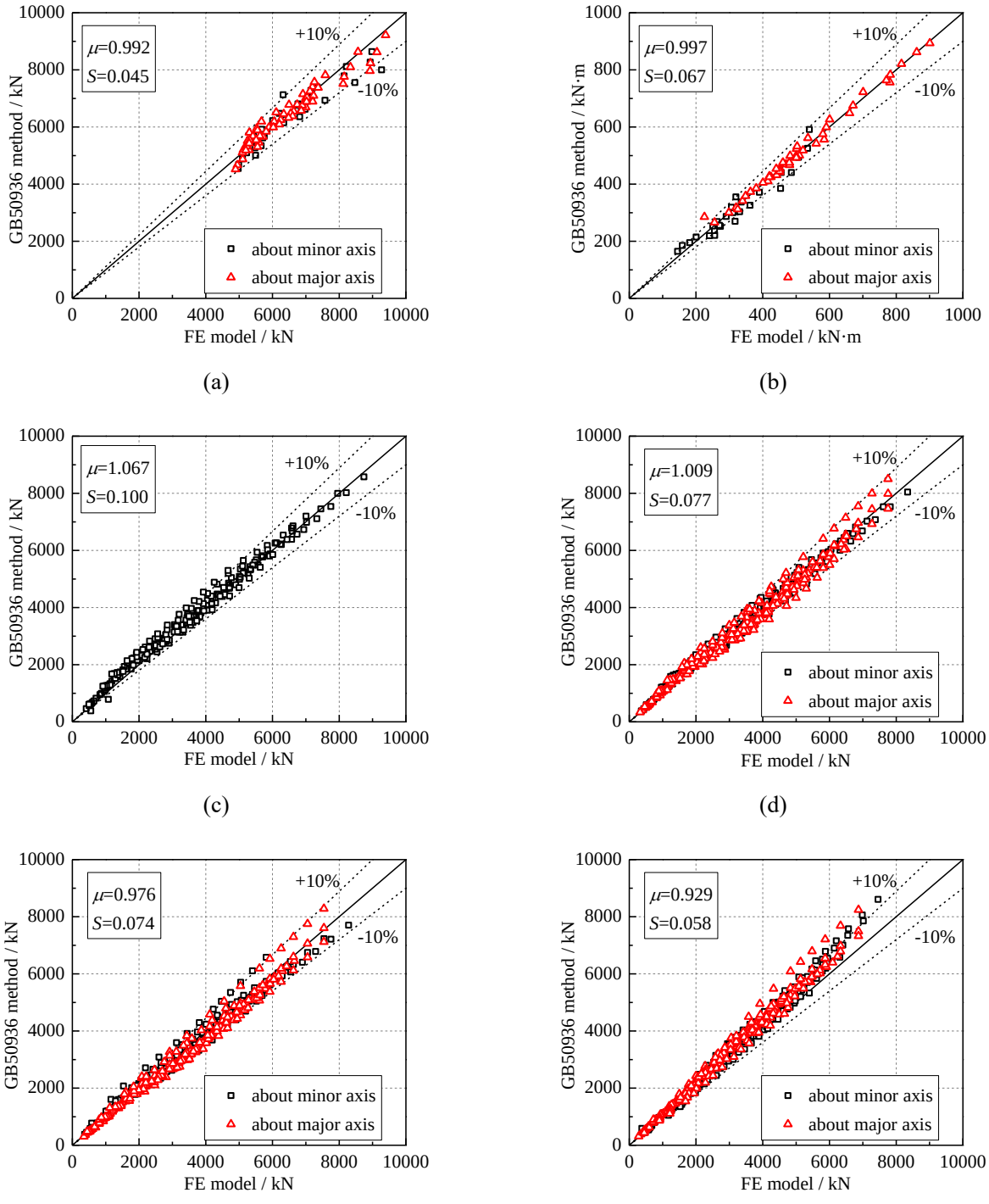

Fig.13 Comparisons between predicted results of GB50936 and FE results: (a) axial compression; (b) bending; and combined compression and bending: (c) $a=b$; (d) $a=1.5b$; (e) $a=2b$; and (f) $a=2.5b$.

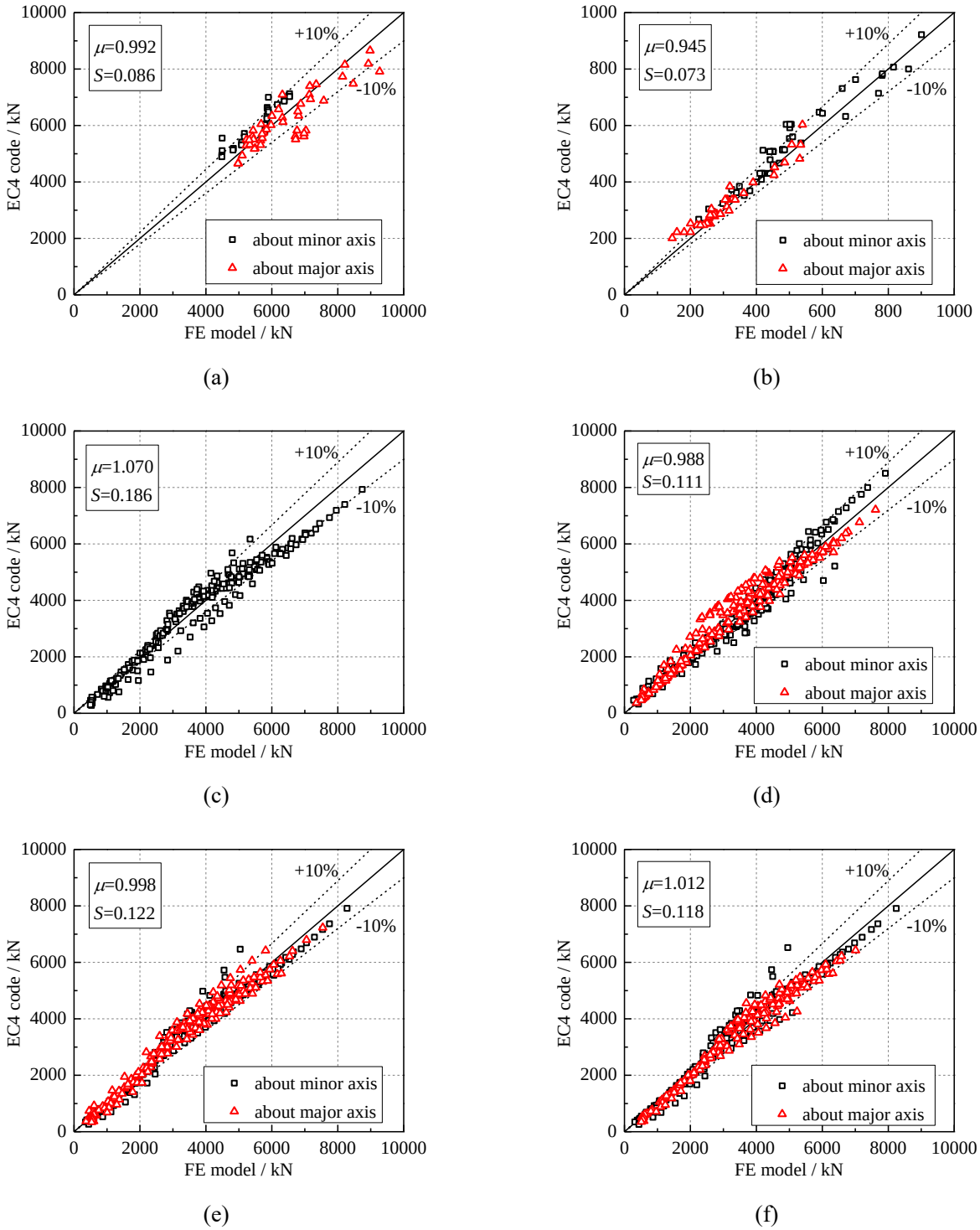

Fig.14 Comparisons between predicted results of EC4 and FE results: (a) axial compression; (b) bending; and combined compression and bending: (c) $a=b$; (d) $a=1.5b$; (e) $a=2b$; and (f) $a=2.5b$.

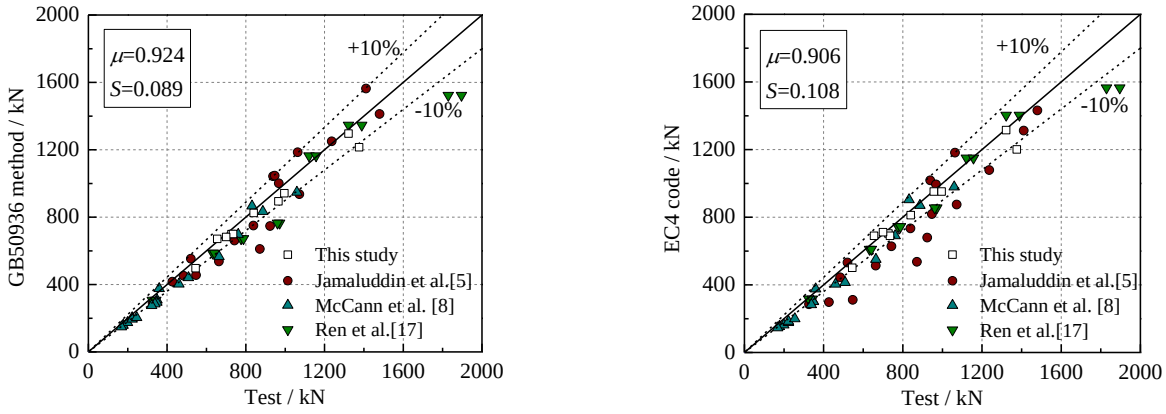

(a) (b)

Fig.15 Comparisons between predicted results of design methods and test results: (a) GB50936; and (b) EC4.

Table 1 Ranges of parameters from previous studies

Fabrication method	Member	Reference	$2a$ (mm)	$2b$ (mm)	a/b	t_s (mm)	α_s (%)	L (mm)	e (mm)	Buckling axis	Number of specimens
Hot-finished	stub column	Yang et al.[2]	150	75	2.0	4, 5, 6.3	18.2, 23.6, 31.2	300	0	-	21
		Zhao and Packer [3]	150	75	2.0	4, 5, 6.3	18.2, 23.6, 31.2	500	0	-	12
			200	100	2.0	5, 6.3, 8, 10	17.0, 22.1 29.4, 38.9	600			
			220	110	2.0	6	18.7	698			
			320	160		8	17.0	-			
		Jamaluddin et al. [5]	150	75	2.0	4.0	18.2	$4a$	0	-	6
			200	100		5.0	17.0				
	slender column	Jamaluddin et al. [5]	150	75	2.0	4.0	18.2	λ=16-143	0	Minor	18
			200	100		5.0	17.0				
		Mahgub et al. [9]	150	75	2.0	6.3	31.2	1500, 2000, 2500	0	Minor	8
			250	125			17.1	2000			
	slender column (fire)	Ali et al. [11]	200	100	2.0	8	29.4	1800	0	Minor	3
		Ali et al. [12]	200	100	2.0	8	29.4	1800	0	Minor	9
			300	150			18.2				
			400	200			13.2				
	beam-column	Sheehan et al. [6]	150	75	2.0	6.6, 4.8	33.2, 22.8	300	25, 75, 100	Minor & Major	8
		McCann et al. [8]	150	75	2.0	6.3	31.2	1154, 2154, 3154, 300 (stub)	0-$2a$ 0-1.33b	Minor & Major	27

Cold-formed	stub column	Uenaka [15]	160	107 80 64	1.5 2.0 2.5	1.0 1.6 2.3	3.2-10.9	160, 200, 250	0	-	21
		Chan et al. [16]	120	60	2.0	5, 8	30.9, 57.3	250	0	-	6
		Liu et al. [21]	135.3 169.2 203.3 237.5 318 139.6	135.3 112.8 101.6 95 159 69.8	1.0 1.5 2.0 2.5	2.75	8.0 5.0 12.0	4*a*	0	-	18
	beam-column	Ren et al. [17]	192	124	1.5	3.8	11.0	λ=38, 56, 75	0, 48, 144	Major	14
	beam-column (fire)	Espinos et al. [20]	220	110	2.0	12	43.6	2135	0, 20, 50	Minor	6
	beam	Ren et al. [17]	192	124	1.5	3.8	11.0	-	-	Major	6
		Uenaka and Tsunokake [18]	160	80	2.0	1.0 1.6 2.3	3.9 6.3 9.2	-	-	Minor & Major	6
		Uenaka and Tsunokake [19]	160	80	2.0	1.0 1.6 2.3	3.9 6.3 9.2	-	-	Minor & Major	6

Table 2 Detailed parameters of the specimens

Column No.	$2a$ (mm)	$2b$ (mm)	t_s (mm)	Specimen length L (mm)	L_e (mm)	a/b	α_s (%)	e_z (mm)	Nominal λ	Buckling axis
S-8-0	201.2	101.2	2.59	407	407	1.99	8.2	0	-	-
S-8-25	200.0	101.2	2.59	407	537.4	1.98	8.2	25	8	Major
S-8-50	202.1	101.1	2.59	407	537.4	2.00	8.2	50	8	Major
L-Ma-35-0	203.3	105.9	2.63	1780	1910.4	1.92	8.0	0	35	Major
L-Ma-35-25	203.3	103.1	2.59	1780	1910.4	1.97	8.0	25	35	Major
L-Ma-35-50	202.7	105.0	2.62	1780	1910.4	1.93	8.0	50	35	Major
L-Ma-50-0	199.7	105.7	2.60	2540	2670.4	1.89	8.0	0	50	Major
L-Ma-50-25	201.3	103.3	2.61	2540	2670.4	1.95	8.1	25	50	Major
L-Ma-50-50	201.3	103.7	2.62	2540	2670.4	1.94	8.1	50	50	Major
L-Mi-70-0	204.3	103.1	2.60	1780	1910.4	1.98	8.1	0	70	Minor
L-Mi-100-0	200.3	103.3	2.59	2540	2670.4	1.94	8.1	0	100	Minor

Table 3 Comparisons between FE and test load-carrying capacity

Column No.	$N_{u,test}$ (kN)	$N_{u,FE}$ (kN)	$N_{u,FE}$ / $N_{u,test}$
S-8-0	1322	1276	0.97
S-8-25	996	912	0.92
S-8-50	736	680	0.92
L-Ma-35-0	1376	1115	0.81
L-Ma-35-25	840	772	0.92
L-Ma-S35-50	655	551	0.84
L-Ma-50-0	1140	1015	0.89
L-Ma-50-25	700	651	0.93
L-Ma-50-50	545	477	0.88
L-Mi-70-0	966	884	0.92
L-Mi-100-0	728	620	0.85
Mean			0.90
Standard Deviation			0.047